Resonance of hypernuclei with complex momentum representation*

Hantao Zhang (张涵韬)[1] C.F. Chen (陈超锋)[1†] Xian-Rong Zhou (周先荣)[2] Zhongzhou Ren (任中洲)[1,3‡]

[1]School of Physics Science and Engineering, Tongji University, Shanghai 200092, China
[2]School of Physics and Electronic Science, East China Normal University, Shanghai 200241, China
[3]Key Laboratory of Advanced Micro-Structure Materials, Ministry of Education, Shanghai 200092, China

Abstract: By combining the Skyrme-Hartree-Fock method with complex momentum representation (CMR), the resonant states of ${}^{17}_{\Lambda}$O, ${}^{41}_{\Lambda}$Ca, ${}^{49}_{\Lambda}$Ca, and ${}^{57}_{\Lambda}$Ni are investigated. The phase shifts for hyperon-nucleus elastic scattering are determined with continuum level density (CLD) and the scatting length as well as the resonance energy are obtained by utilizing the effective range expansion. Our method abbreviated as CMR-CLD exhibits good consistency with traditional approaches and provides some ground work for investigating scattering and resonance problems in deformed hypernuclei and multi-hyperon hypernuclei.

Keywords: resonance, complex momentum representation, hypernuclei

DOI: **CSTR:**

CPC Accepted

I. INTRODUCTION

Hypernuclear system is an important research subject in nuclear physics, and significant studies have been conducted in production, decay and structure of hypernuclei. Various theoretical works have also been proposed to investigate different aspects of the nature of hypernuclei, such as the generator coordinate method (GCM) [1, 2], the orthogonality condition model [3−5], the Tohsaki-Horiuchi-Schuck-Röpke (THSR) wave function [6−9], the variational Monte Carlo (VMC) method [10], the Gaussian expansion method [11−18], the cluster orbit shell model [19], the particle rotor model [20], the mean-field approaches [21−33] and so on.

In hypernuclear physics one of the main aspects is to study the new dynamical and structural properties by an addition of a hyperon (or few hyperons). Because of the absence of the Pauli principle between nucleons and the hyperon, participation of the hyperon in nuclei leads to stronger effect of attraction and thus possibly more bound states and may change the location of the drop line. The contraction of the nuclear cores will be significant and such phenomena are called as ‘glue-like’ role of the hyperon. The systematic study of binding energy of light single hyperon-hypernuclei has traditionally been a key topic, which has been investigated for stable nuclei and neutron-rich nuclei plus hyperons.

Another important subject in hypernuclear physics is to investigate the hyperon-nucleon and hyperon-nucleus scattering process and find new resonant states due to the injection of the hyperon. For addressing the resonance problems many theoretical approaches have been proposed and applied successfully to handle resonant states and scattering process, such as the *R*-matrix method [34−38], the complex scaling method (CSM) [39−46], the complex momentum representation (CMR) [47−52], the trap method [53−64] and so on.

As a mean-field approach, the Skyrme-Hartree-Fock (SHF) method [27−33] is based on the self-consistent Hartree-Fock equations and uses the Skyrme potential for the nucleon-nucleon interaction. It has been successfully applied to the study of nuclear structure, deformation, energy spectrum and so on. By extending SHF with various hyperons, it has also been effectively utilized in hypernuclear research. For light hypernuclei, in addition to few-body methods and microscopic cluster models, SHF can still be effective when one is interested in the binding energy of hyperons. In this case, the deviations arising from the limitations of the mean-field approximation and corresponding inadequate description of nuclear parts are partially compensated [29], allowing SHF to be applied across a wide mass range, from light to heavy hypernuclei.

In this work, we combine Skyrme-Hartree-Fock

Received 3 September 2024; Accepted 5 December 2024

* This work is supported by the National Natural Science Foundation of China (Grants No. 12035011, No. 11905103, No. 11947211, No. 11761161001, No. 11961141003, No. 12022517 and No. 12375122), by the National Key R&D Program of China (Contracts No. 2023YFA1606503), by the Science and Technology Development Fund of Macau (Grants No. 0048/2020/A1 and No. 008/2017/AFJ), by the Fundamental Research Funds for the Central Universities (Grant No. 22120210138 and No. 22120200101)

† E-mail: cfchen@tongji.edu.cn
‡ E-mail: zren@tongji.edu.cn

©2025 Chinese Physical Society and the Institute of High Energy Physics of the Chinese Academy of Sciences and the Institute of Modern Physics of the Chinese Academy of Sciences and IOP Publishing Ltd. All rights, including for text and data mining, AI training, and similar technologies, are reserved.

method with complex momentum representation to address the resonant state problem of spherical nuclei plus single Λ hyperon. Hyperon scattering experiments are crucial for investigating and understanding hyperon-nucleon interactions and also baryon-baryon interactions. Although experimental data related to hyperon-nucleus scattering is currently lacking, we have derived some predictions for these experimental data based on our theoretical methods.

Specifically speaking, we combine CMR with continuum level density (CLD) [38, 65, 66] to calculate the scattering phase shifts between hyperon and nuclear core, and extract the scattering length from the scattering phase shifts obtained from CMR-CLD based on effective range expansion [67, 68]. The numerical results obtained through our methods show good consistency with those from traditional methods, which provides some valuable insights for studying resonance and scattering in hypernuclei within the mean-field and complex momentum representation frameworks.

The rest of the article is organized as follows: In Sec.II, we first formulate the Skyrme-Hartree-Fock framework incorporating hyperons. Next, we present the theoretical frameworks for complex momentum representation, continuum level density, and effective range expansion. In Sec.III the numerical results for single Λ hyperon and spherical nuclear core scattering are presented and discussed. Sec.IV summarizes the article.

II. THEORETICAL FORMALISM

A. Skyrme-Hartree-Fock method

The total energy of a single-hyperon hypernucleus can be written as [69–71]

$$E = \int \mathrm{d}^3\boldsymbol{r}\varepsilon(\boldsymbol{r}), \quad \varepsilon = \varepsilon_{NN} + \varepsilon_{\Lambda N}, \tag{1}$$

where ε_{NN} and $\varepsilon_{\Lambda N}$ account for the nucleon-nucleon and hyperon-nucleon interactions, respectively. The energy-density functional depends on the one-body density $\rho_q(\boldsymbol{r})$, kinetic density $\tau_q(\boldsymbol{r})$, and spin-orbit current $\boldsymbol{J}_q(\boldsymbol{r})$,

$$\begin{aligned}
\rho_q(\boldsymbol{r}) &= \sum_{i=1}^{N_q} n_q^i \left|\phi_q^i(\boldsymbol{r})\right|^2, \\
\tau_q(\boldsymbol{r}) &= \sum_{i=1}^{N_q} n_q^i \left|\nabla\phi_q^i(\boldsymbol{r})\right|^2, \\
\boldsymbol{J}_q(\boldsymbol{r}) &= \sum_{i=1}^{N_q} n_q^i \phi_q^{i*} \left(\nabla\phi_q^i(\boldsymbol{r})\times\sigma\right)/i,
\end{aligned} \tag{2}$$

where ϕ_q^i $(i = 1,...N_q)$ are self-consistently calculated the single-particle wave functions of the N_q occupied states for the different particles q =n, p, and Λ. They satisfy the Schrödinger equation, obtained by the minimization of the total energy functional Eq. (1) according to the variational principle,

$$\left[\nabla\cdot\frac{1}{2m_q^*(\boldsymbol{r})}\nabla - V_q(\boldsymbol{r}) + i\boldsymbol{W}_q(\boldsymbol{r})\cdot(\nabla\times\boldsymbol{\sigma})\right]\phi_q^i(\boldsymbol{r}) = e_q^i\phi_q^i(\boldsymbol{r}), \tag{3}$$

in which $\boldsymbol{W}_q(\boldsymbol{r})$ is the spin–orbit interaction part for the nucleons as given in Refs. [72], while the spin-orbit force for the Λ hyperon is very small [73, 74] and it is ignored in the present study. The central mean-fields $V_q(\boldsymbol{r})$, corrected by the effective-mass terms following the procedure described in Refs.[69, 71] are

$$\begin{aligned}
V_N = V_N^{\mathrm{SHF}} &+ \frac{\partial\varepsilon_{N\Lambda}}{\partial\rho_N} \\
&+ \frac{\partial}{\partial\rho_N}\left(\frac{m_\Lambda}{m_\Lambda^*(\rho_N)}\right)\left(\frac{\tau_\Lambda}{2m_\Lambda} - \frac{3}{5}\frac{\rho_\Lambda\left(3\pi^2\rho_\Lambda\right)^{2/3}}{2m_\Lambda}\right),
\end{aligned} \tag{4}$$

$$V_\Lambda = \frac{\partial\varepsilon_{N\Lambda}}{\partial\rho_\Lambda} - \left(\frac{m_\Lambda}{m_\Lambda^*(\rho_N)} - 1\right)\frac{\left(3\pi^2\rho_\Lambda\right)^{2/3}}{2m_\Lambda}. \tag{5}$$

The Skyrme force SLy5 [75, 76] is used for the nucleon-nucleon interaction ε_{NN}, and the hyperon-nucleon interaction $\varepsilon_{N\Lambda}$ is parameterized as (densities ρ given in units of fm^{-3}, energy density ε in MeV fm $^{-3}$):

$$\begin{aligned}
\varepsilon_{N\Lambda}(\rho_N,\rho_\Lambda) = &-\left(\varepsilon_1 - \varepsilon_2\rho_N + \varepsilon_3\rho_N^2\right)\rho_N\rho_\Lambda \\
&+ \left(\varepsilon_4 - \varepsilon_5\rho_N + \varepsilon_6\rho_N^2\right)\rho_N{\rho_\Lambda}^{5/3},
\end{aligned} \tag{6}$$

together with

$$\frac{m_\Lambda^*}{m_\Lambda}(\rho_N) \approx \mu_1 - \mu_2\rho_N + \mu_3\rho_N^2 - \mu_4\rho_N^3. \tag{7}$$

The parameter $\varepsilon_1,...,\varepsilon_6$ in Eq. (6) and the Λ effective-mass μ_i were determined in BHF calculations with the Nijmegen potential NSC97f [71, 77].

B. Complex momentum representation (CMR)

The nuclear cores considered in this work are almost spherical and the deformation can be neglected, therefore, the single channel Schrödinger equation in momentum representation can be written as:

$$\frac{\hbar^2k^2}{2\mu}\phi(k) + \int V_l(k,k')\phi(k')k'^2dk' = E\phi(k), \tag{8}$$

CPC Accepted

where the reduced mass $\mu = \frac{Am_N m_\Lambda}{Am_N + m_\Lambda}$ with A being the nucleon number of nuclear core, nucleon mass m_N being 938.918 MeV and Λ hyperon mass m_Λ being 1115.683 MeV. The potential in momentum space $V_l(k,k')$ is obtained by the spherical potential $V(r)$ extracted from the Skyrme-Hartree-Fock method:

$$V_l(k,k') = \frac{2}{\pi}\int j_l(kr)V(r)j_l(k'r)r^2dr, \tag{9}$$

where j_l represents the spherical Bessel function. Although the doubly-magic core nuclei considered in this work do exhibit deformation experimentally, the deformation is relatively small and these core nuclei can be regarded as near-spherical nuclei. Therefore, we employ a spherical hyperon-nucleus interaction $V(r)$ in our theoretical framework. When deformation cannot be neglected, Eq.(8) will become a coupled equation.

As mentioned, we can extract effective potential $V(r)$ between the nucleus and the single hyperon from SHF calculations, explicitly speaking, from the nucleon and hyperon density distributions. In this work, we select the Skyrme force SLy5 for nucleon-nucleon interaction and the Nijmegen potential NSC97f for hyperon-nucleon interaction. The Nijmegen potential NSC97f is chosen because it can successfully describe the binding energy of single hyperon in hypernuclei and also effectively accounts for the binding energy of multiple hyperons in multi-hyperon hypernuclei [30]. The SLy5 interaction is selected for nucleon-nucleon interactions due to its good performance in describing nuclear structure [75, 76]. Additionally, once the hyperon-nucleon interaction is determined, the choice of nucleon-nucleon interaction has a insignificant impact on the binding energies of hyperons [24].

The integral function (8) can be converted into a equivalent matrix equation involving the summation over a finite set of mesh points k_i in momentum space:

$$\frac{\hbar^2 k_i^2}{2\mu}\phi(k_j)\delta_{i,j} + \sum_j V_l(k_i,k_j)\phi(k_j)k_j^2\omega_j = E\phi(k_i), \tag{10}$$

where ω_j represents the weight of j-th momentum mesh point. In our calculations the complex Gaussian-Legendre mesh is adopted and our contours consist of line segments in complex momentum space. Generally speaking, as long as the contour can enclose the discrete eigenstates we wish to obtain and the momentum cutoff k_{max} is sufficiently large, the shape of the contour has no effect on the final calculation result.

In addition, one can also find that the contour $ke^{-i\theta}$ is exactly equivalent to complex scaling in coordinate space:

$$U(\theta)f(\mathbf{r}) = \exp(i\frac{3}{2}\theta)f(\mathbf{r}\exp(i\theta)). \tag{11}$$

However, when excessively large complex scaling angles are employed in the complex scaling method, the computation will become unstable. However, this issue does not exist for CMR. Therefore, CMR can exhibit better computational performance for broader resonant states.

In this work, we only address the resonance states of spherical hypernuclei through CMR. In the more general case of deformed potentials, coupling effects of higher excited energy levels could be very crucial, which is essential for analyzing deformed hypernuclei. Moreover, extending CMR to coupled-channel problems is also straightforward and convenient, which allows us to further discuss the impact of deformation effects on hyperon emission.

C. Continuum level density (CLD)

1. *CLD*

The level density $\rho(\varepsilon)$ of the full Hamiltonian h is defined by:

$$\rho(\varepsilon) = \sum_i \!\!\!\!\!\!\int \delta(\varepsilon - \varepsilon_i), \tag{12}$$

where ε_i are eigenvalues of h, summation and integration are taken for discrete and continuous eigenvalues, respectively. This definition of the level density can also be expressed with the help of the Green's function:

$$\rho(\varepsilon) = -\frac{1}{\pi}\mathrm{Im}\left\{\mathrm{Tr}\left[\frac{1}{\varepsilon + i0 - h}\right]\right\}. \tag{13}$$

When the Hamiltonian is described by a sum of an asymptotic term h_0 and the short-range interaction V, namely $h = h_0 + V$, the CLD (denoted by $\Delta(\varepsilon)$) for an energy ε is expressed with the density $\rho(\varepsilon)$ obtained from the full Hamiltonian h and the level density $\rho_0(\varepsilon)$ of continuum states obtained from the asymptotic Hamiltonian h_0 as:

$$\begin{aligned}\Delta(\varepsilon) &= \rho(\varepsilon) - \rho_0(\varepsilon) \\ &= -\frac{1}{\pi}\mathrm{Im}\left[\mathrm{Tr}\left\{\frac{1}{\varepsilon + i0 - h} - \frac{1}{\varepsilon + i0 - h_0}\right\}\right].\end{aligned} \tag{14}$$

Additionally, $\Delta(\varepsilon)$ is well known to be related to the scattering S-matrix $S(\varepsilon)$ as:

$$\Delta(\varepsilon) = \frac{1}{2\pi}\mathrm{Im}\frac{d}{d\varepsilon}\ln\{\det S(\varepsilon)\}, \tag{15}$$

CPC Accepted

for a single channel system, the scattering S-matrix can be expressed as: $S(\varepsilon)=e^{2i\delta(\varepsilon)}$, where $\delta(\varepsilon)$ is the scattering phase shift. In such case we can obtain the simplified CLD and the scattering phase shift

$$\Delta(\varepsilon)=\frac{1}{\pi}\frac{d\delta}{d\varepsilon},\quad \delta(\varepsilon)=\pi\int_{-\infty}^{\varepsilon}\Delta(\varepsilon')d\varepsilon'. \tag{16}$$

2. *CMR-CLD*

If the energy spectrum is obtained through N momentum mesh points in the CMR. The CMR-CLD can be expressed in the following form:

$$\begin{aligned}\Delta_N^{CMR}(\varepsilon)=&\sum_b^{N_B}\delta(\varepsilon-\varepsilon_b)+\frac{1}{\pi}\sum_r^{N_R^{CMR}}\frac{\Gamma_r/2}{(\varepsilon-\varepsilon_r)^2+\Gamma_r^2/4}\\&+\frac{1}{\pi}\sum_C^{N_C^{CMR}=N-N_B-N_R^{CMR}}\frac{\epsilon_C^I}{(\varepsilon-\epsilon_C^R)^2+\epsilon_C^{I\,2}}\\&-\frac{1}{\pi}\sum_C^{N}\frac{\epsilon_C^{0I}}{(\varepsilon-\epsilon_C^{0R})^2+\epsilon_C^{0I\,2}},\end{aligned} \tag{17}$$

where ε_b, $\varepsilon_r-i\Gamma_r/2$ and $\epsilon^R-i\epsilon^I$ are eigenvalues of the full Hamiltonian $h=T+V$, $\epsilon^{0R}-i\epsilon^{0I}$ are eigenvalues of asymptotic Hamiltonian $h_0=T$. N_B represents the number of the bound state and N_R^{CMR} represents the number of the resonant state.

With Eq.(16) the phase shift within the N complex momentum mesh points in the CMR can be expressed as:

$$\begin{aligned}\delta_N^{CMR}(\varepsilon)=&\pi\int_{-\infty}^{\varepsilon}\Delta_N^{CMR}(\varepsilon)\\=&N_B\pi+\sum_{r=1}^{N_R^{CMR}}\int_0^{\varepsilon}d\varepsilon\frac{\Gamma_r/2}{(\varepsilon-\varepsilon_r)^2+\Gamma_r^2/4}\\&+\int_0^{\varepsilon}d\varepsilon[\sum_{C=1}^{N_C^{CMR}}\frac{\epsilon_C^I}{(\varepsilon-\epsilon_C^R)^2+\epsilon_C^{I\,2}}-\sum_{C=1}^{N}\frac{\epsilon_C^{0I}}{(\varepsilon-\epsilon_C^{0R})^2+\epsilon_C^{0I\,2}}]\\=&N_B\pi+\delta_R(\varepsilon)+\delta_C(\varepsilon),\end{aligned} \tag{18}$$

where the resonance and non-resonance phase shifts are given as:

$$\delta_R(\varepsilon)=\sum_{r=1}^{N_R^{CMR}}\delta_r(\varepsilon),\quad \delta_C(\varepsilon)=\sum_{c=1}^{N_C^{CMR}}\delta_c(\varepsilon)-\sum_{c=1}^{N}\delta_c^0(\varepsilon). \tag{19}$$

3. *Effective range expansion (ERE)*

Using the continuum level density, the scattering phase shifts can be conveniently obtained from the energy spectrum. To extract the information such as scattering length, effective range, resonance energies and so on from the phase shifts, we choose the effective range expansion to expand the phase shift δ_l through a power series in momentum k:

$$\begin{aligned}&C_l^2(\eta)k^{2l+1}\left[\cot(\delta_l)+\frac{2\eta H(\eta)}{C_0^2(\eta)}\right]\\&=-\frac{1}{a_l}+\frac{r_lk^2}{2}+P_lr_l^3k^4+O(k^6),\end{aligned} \tag{20}$$

where a_l is the scattering length, r_l is the effective range, and P_l is the shape parameter of partial wave l. In this expression $C_l^2(\eta)$, $C_0^2(\eta)$ and $H(\eta)$ are given by:

$$\begin{aligned}&C_l^2(\eta)=C_{l-1}^2(\eta)(1+\frac{\eta^2}{l^2}),\ C_0^2(\eta)=\frac{2\pi\eta}{e^{2\pi\eta}-1},\\&H(\eta)=\sum_{s=1}^{\infty}\frac{\eta^2}{s(s^2+\eta^2)}-\ln(\eta)-\gamma\\&\quad=-\frac{i\pi}{e^{2\pi\eta}-1}+\Psi(i\eta)+\frac{1}{2i\eta}-\ln(i\eta),\end{aligned} \tag{21}$$

where $\eta=\dfrac{Z_1Z_2e^2\mu}{\hbar^2k}$, $\gamma=0.5772156649\cdots$ is the Euler's constant, $\Psi(z)$ is the logarithmic derivative of the Γ function (Ψ function or digamma).

In the case of neutral particle scattering, the effective range expansion reads:

$$k^{2l+1}\cot(\delta_l)=-\frac{1}{a_l}+\frac{r_lk^2}{2}+P_lr_l^3k^4+O(k^6). \tag{22}$$

According to the form of the on-shell elements of T-matrix: $T(k,k)=\dfrac{(4\pi)^2}{2\mu k}\dfrac{1}{\cot(\delta_l(k))-i}$, one can find that the resonance is the pole of the T-matrix and thus phase shift at complex momentum $k_{res}=\dfrac{\sqrt{2\mu E_{res}}}{\hbar}$ of resonant state satisfies the condition $\cot(\delta_l(k_{res}))=i$. Therefore, through effective range expansion, the parametrization of the phase shift at k_{res} satisfies the following equation:

$$-\frac{1}{a_l}+\frac{r_lk^2}{2}+P_lr_l^3k^4+O(k^6)=C_l^2(\eta)k^{2l+1}\left[i+\frac{2\eta H(\eta)}{C_0^2(\eta)}\right], \tag{23}$$

for neutral particle scattering Eq.(23) becomes:

$$-\frac{1}{a_l}+\frac{r_lk^2}{2}+P_lr_l^3k^4+O(k^6)=ik^{2l+1}. \tag{24}$$

CPC Accepted

III. NUMERICAL RESULTS

Due to the considerably shorter lifetimes observed in hypernuclei compared to those of conventional atomic nuclei, it is thus assumed in studies of hypernuclear resonant states that their cores exist in deeply bound states. Accordingly, stable nuclei such as ^{16}O, ^{40}Ca, ^{48}Ca, and ^{56}Ni have been designated as core nuclei for this purpose. Firstly, from calculations based on Skyrme-Hartree-Fock method, the effective interaction between hyperon and nuclear core can be extracted as $V(r)$. In practical computations only effective potential in a finite region $r < r_{max}$ can be obtained in Skyrme-Hartree-Fock method. To provide potential in the entire coordinate space, we employ a Woods-Saxon form $\frac{V_0}{1+e^{\frac{r-R}{a}}}$ to fit $V(r)$ and utilize the analytical potential beyond r_{max} in Eq.(9).

The effective hyperon-nucleus interactions $V(r)$ for $^{17}_{\Lambda}$O, $^{41}_{\Lambda}$Ca, $^{49}_{\Lambda}$Ca, and $^{57}_{\Lambda}$Ni are plotted in Fig. 1. For these nearly spherical nuclei, the deformation obtained from Skyrme-Hartree-Fock calculations is very small and can be neglected. Hence, we only need to consider single-channel scattering process. However, if the deformation is significant and cannot be ignored, then deformed potentials and the corresponding coupled-channel equations must be considered. It should also be noted that in the current calculations, we assume the energy level splitting induced by spin-orbit coupling is relatively small compared to the energy levels themselves, and thus we have neglected the influence of the spin-orbit coupling potential. However, if a more detailed discussion of the level splitting is required, we can derive a phenomenological spin-orbit coupling potential based on $V(r)$ within the current framework.

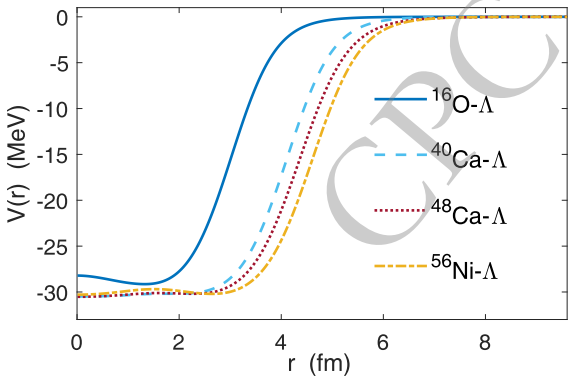

Fig. 1. (color online) The effective potential between the hyperon and the nuclear core extracted from the Skyrme-Hartree-Fock method. Solid, dashed, dotted, and dash-dot line represent the effective potential $V(r)$ for $^{17}_{\Lambda}$O, $^{41}_{\Lambda}$Ca, $^{49}_{\Lambda}$Ca, and $^{57}_{\Lambda}$Ni, respectively.

Table 1. Parameters of the Woods-Saxon potentials. These parameters are derived by fitting the effective interaction obtained from the SHF method with the Woods-Saxon potential. In practical calculations, these parameters are used in the region where $r > r_{max}$.

Hypernuclei	a (fm)	R (fm)	V_0 (MeV)
$^{17}_{\Lambda}$O	0.4264	3.103	−28.75
$^{40}_{\Lambda}$Ca	0.4383	4.128	−30.46
$^{48}_{\Lambda}$Ca	0.4630	4.388	−30.46
$^{56}_{\Lambda}$Ni	0.4438	4.647	−30.18

In the following, we illustrate the results of CMR-CLD and effective rang expansion by taking $^{17}_{\Lambda}$O as an example. In solving the Schrödinger equation in momentum space the truncation of momentum is taken to be $k_{max} = 5$ fm^{-1}, which is large enough to guarantee the stabilization of the numerical solutions. For CMR-CLD, as long as the contour encompasses the discrete eigenvalues, then these discrete eigenvalues are independent on the choice of the contour, furthermore, once the discrete eigenvalues can be accurately solved, the phase shifts obtained through continuum level density also do not depend on the contour shape.

Figure 2 illustrates the complex momentum spectra and phase shifts obtained through CMR-CLD for $^{17}_{\Lambda}$O with orbital angular momentum $l = 0$ and $l = 1$. Both states with $l = 0$ and $l = 1$ are bound states, whose positions are marked on the positive imaginary axis in panel (a). Panel (b) shows the scattering phase shifts obtained with both CMR-CLD and conventional R-matrix method, where circular and square markers represent the P-wave and S-wave phase shifts obtained from R-matrix method, and solid and dashed lines correspond to the P-wave and S-wave phase shifts obtained from CMR-CLD. In the R-matrix calculation of scattering phase shifts, we adopt the conventional Lagrange functions over the interval $(0, a)$, with the channel radius a set to around 20 fm (large enough to neglect the short-range nuclear interaction) and the number of grid points set to about 50. The same parameters are used in the calculation of resonant states.

When considering higher angular momentum, the $l = 2$ state becomes a resonance due to the stronger repulsive centrifugal potential. As shown in Fig. 3(a), a resonance appears in the fourth quadrant of the complex momentum space. The square, diamond, and circular markers in panel (a) represent the complex momentum spectra obtained using three different contour shapes. It can be observed that the position of the resonant state remains almost unchanged regardless of the contour shape. In Fig. 3(b) the phase shifts of $^{17}_{\Lambda}$O for D-wave scattering are displayed, the triangle markers and solid line represent the results obtained by CMR-CLD and R-matrix, respectively. Similar calculations are performed for other systems and we display the phase shifts corresponding to the first resonant state of $^{17}_{\Lambda}$O, $^{41}_{\Lambda}$Ca, $^{49}_{\Lambda}$Ca, and $^{57}_{\Lambda}$Ni in Fig. 4. The solid lines represent results obtained using CMR-

CPC Accepted

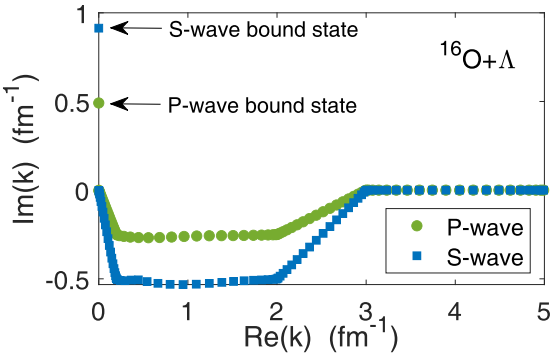

(a) Complex momentum spectrum of S-wave and P-wave for $^{17}_{\Lambda}$O.

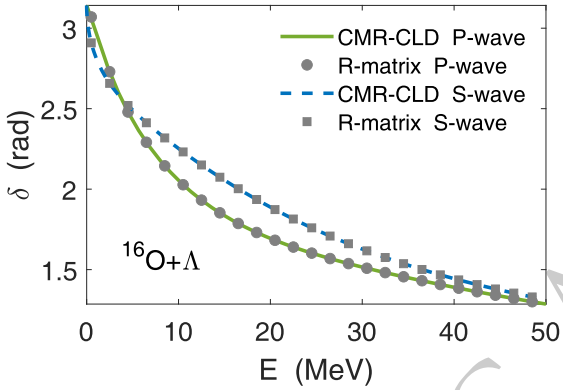

(b) Phase shift of S-wave and P-wave for $^{17}_{\Lambda}$O.

Fig. 2. (color online) (a) The complex momentum spectra of $^{17}_{\Lambda}$O obtained from CMR. The square and circle markers correspond to the results for S-wave and P-wave, respectively. Two bound states are marked on the positive imaginary axis. (b) The phase shifts of $^{17}_{\Lambda}$O for S-wave and P-wave. The square and circle markers represent the phase shifts obtained by R-matrix method for S-wave and P-wave, respectively. The dashed and solid lines represent the phase shifts obtained by CMR-CLD for S-wave and P-wave, respectively.

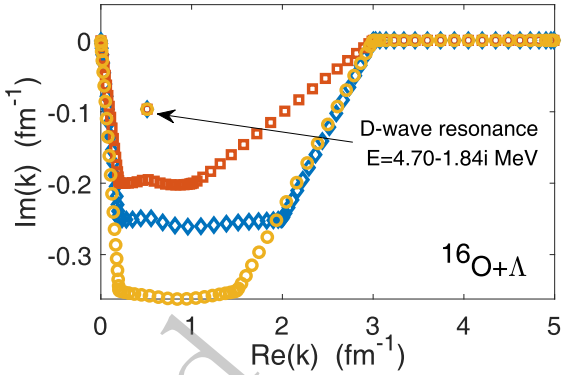

(a) Complex momentum spectrum of D-wave for $^{17}_{\Lambda}$O.

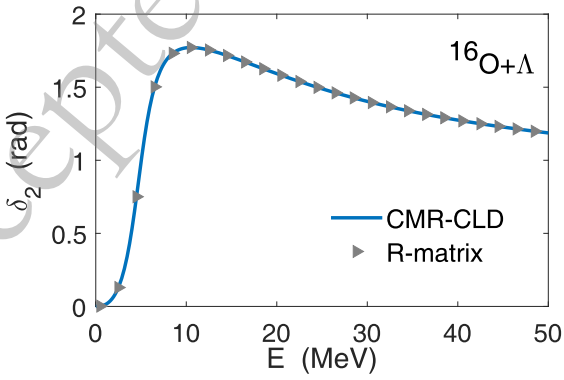

(b) Phase shift of D-wave for $^{17}_{\Lambda}$O.

Fig. 3. (color online) (a)The complex momentum spectra of $^{17}_{\Lambda}$O obtained from CMR. The square, circle and rhombus markers correspond to three different contours. The D-wave resonant state and its eigenenergy are marked in this panel. (b) The phase shifts of $^{17}_{\Lambda}$O for D-wave. The triangle markers represent the phase shifts obtained by R-matrix and the solid line represent the results obtained by CMR-CLD.

CLD, while the markers denote results obtained with the R-matrix method.

After obtaining the phase shifts through CMR-CLD, we can also extract physical quantities such as scattering length, complex resonant energy by using effective range expansion. For the D-wave scattering of $^{17}_{\Lambda}$O, these extracted physical quantities are listed in Table 2. For other systems, the calculations are similar and the corresponding results are also listed in Table 2.

The first column represents the nuclear core, the second column denotes the angular momentum l which supports the first resonant state, the third column indicates the scattering length a_l obtained from CMR-CLD with effective range expansion, the fourth column displays the scattering length obtained from the R-matrix method, the fifth column shows the complex resonant energy E_{res} obtained from the R-matrix method and the

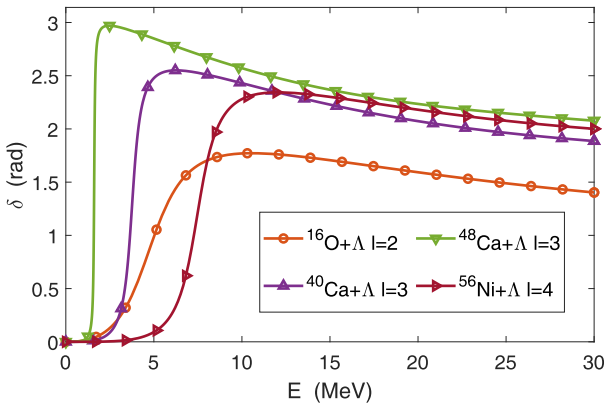

Fig. 4. (color online) The scattering phase shifts at the appearance of the first resonant state. Solid lines represent the calculations from CMR-CLD, while circle, square, diamond, upward triangle, downward triangle, and right triangle markers correspond to the results of R-matrix method for $^{17}_{\Lambda}$O, $^{41}_{\Lambda}$Ca, $^{49}_{\Lambda}$Ca, and $^{57}_{\Lambda}$Ni, respectively.

CPC Accepted

Table 2. The complex resonant energy E_{res} and scattering length a_l computed with CMR-CLD and R-matrix method. Here, the angular momentum l supports the first resonant state. $a_l^{CMR-CLD+ERE}$ and $E_{res}^{CMR-CLD+ERE}$ denote the scattering length and resonant energy obtained from CMR-CLD plus effective range expansion, respectively. E_{res}^{CMR} is the result calculated from pure CMR. Here, "pure" refers to extracting resonant energies solely from the momentum spectrum obtained from CMR. To ensure reliable resonance extraction, we have carefully selected an appropriate integral contour. $a_l^{R-matrix}$ and $E_{res}^{R-matrix}$ denote the scattering length and resonant energy obtained from R-matrix method, respectively. In the R-matrix calculations, the channel radius is set to be around 20 fm and about 50 Gaussian-Legendre grid points are used.

Nuclear core	l	$a_l^{CMR-CLD+ERE}$ (fm^{2l+1})	$a_l^{R-matrix}$ (fm^{2l+1})	$E_{res}^{R-matrix}$ (MeV)	$E_{res}^{CMR-CLD+ERE}$ (MeV)	E_{res}^{CMR} (MeV)
^{16}O	2	−16.50	−16.49	4.70-1.84i	4.70-1.84i	4.70-1.84i
^{40}Ca	3	−53.02	−53.03	3.76-0.387i	3.76-0.387i	3.76-0.387i
^{48}Ca	3	−181.0	−180.9	1.61-0.0408i	1.61-0.0406i	1.61-0.0408i
^{56}Ni	4	−30.93	−30.98	7.46-0.951i	7.46-0.954i	7.46-0.951i

sixth column shows E_{res} obtained from CMR-CLD plus effective range expansion, and E_{res} obtained by CMR are listed in the last column.

Generally speaking, the positive or negative phase shift at a certain scattering energy indicates whether the interaction is attractive or repulsive. Due to the connection between phase shift $\delta_l(k)$ and scattering length a_l, namely $\lim\limits_{k\to 0}\dfrac{k^{2l+1}}{\tan(\delta_l(k))}=-\dfrac{1}{a_l}$, a negative scattering length corresponds to a positive scattering phase shift near zero energy, which indicates an attractive effect in this energy region, while a positive scattering length reflects a repulsive effect on the contrary. Moreover, qualitatively speaking, the larger (in absolute value) the scattering length, the stronger the attractive (or repulsive) effect near zero energy. This can also be partially reflected from Table 2: the larger absolute values of the scattering length correspond to smaller decay widths, namely indicating stronger attractive effect between Λ hyperon and nuclear core. However, it should be noted that such comparison should be based on the condition of equal angular momentum and thus the magnitude of scattering lengths can not be directly compared for different angular momentum cases.

From Table 2, it is evident that the complex resonant energy obtained through CMR closely matches those obtained from the conventional R-matrix method. Additionally, the scattering length and complex resonant energy extracted through effective range expansion also exhibit good agreement with results obtained from the R-matrix method. These numerical results validate the reliability and accuracy of the CMR-CLD method in dealing with resonance problems for single hyperon hypernuclei in the case of spherical potential.

From the numerical results, we can find that for the single Λ hypernuclei considered, the decay width is approximately in the MeV range, which is much larger than the decay width derived from the weak decay lifetime of hypernucleus. Therefore, this indicates that the time involved in the emission process within the hypernucleus is much shorter than its weak decay lifetime and also much shorter than the half-life of a free Λ hyperon. These results suggest that even if the weak decay lifetime of the hypernucleus is pretty short, the emission process of the hyperon should also be considered and investigated.

IV. CONCLUSIONS

We combine Skyrme-Hartree-Fock method with complex momentum representation to investigate the resonances of single hyperon hypernuclear and obtain the complex resonant energy through solving the single channel Schrödinger equation in complex momentum space. CMR offers the advantage of employing bound state techniques to address resonances, moreover, when considering deformed potentials, CMR can be easily extended to coupled-channel sectors. Then the influence of deformation effects on hyperon emission can be further discussed in the future. In the present work, through selecting appropriate momentum cutoff and contour for integral the resonance energies obtained from CMR are highly consistent with the results from R-matrix methods. In addition, based on the continuum level density method the phase shifts are calculated with energy spectrum obtained from CMR. The scattering phase shifts from CMR-CLD are in good agreement with those from R-matrix method. Additionally, by applying effective range expansion, we also extract the reliable scattering length, from which we can obtain information about the strength of the attractive interaction between the hyperon and the nuclear core during the scattering process.

Our study of the spherical nuclear system with a single hyperon demonstrates the good reliability of the CMR-CLD method, which lays a foundation for future investigations using CMR-CLD to study resonant states in deformed single hyperon hypernuclei and multi-hyperon hypernuclei.

CPC Accepted

References

[1] H. Bandō, M. Seki, and Y. Shōno, Prog. Theor. Phys. **66**, 2118 (1981)
[2] T. Yamada, K. Ikeda, H. Bandō, and T. Motoba, Prog. Theor. Phys. **73**, 397 (1985)
[3] T. Motoba, H. Bandō, and K. Ikeda, Prog. Theor. Phys. **70**, 189 (1983)
[4] W. Xi-cang, H. Takaki, and H. Bandō, Prog. Theor. Phys. **76**, 865 (1986)
[5] W. Xi-cang, H. Bandō, and H. Takaki, Z. Phys. A At. nucl. **327**, 59 (1987)
[6] Y. Funaki, A. Tohsaki, H. Horiuchi, P. Schuck, and G. Röpke, Eur. Phys. J. A **24**, 321 (2004)
[7] Y. Funaki, T. Yamada, E. Hiyama, and K. Ikeda, Nucl. Phys. A **914**, 194 (2013)
[8] Y. Funaki, T. Yamada, E. Hiyama, B. Zhou, and K. Ikeda, Prog. Theor. Exper. Phys. **2014**, 113D (2014)
[9] Y. Funaki, M. Isaka, E. Hiyama, T. Yamada, and K. Ikeda, Phys. Lett. B **773**, 336 (2017)
[10] M. Shoeb, Q. N. Usmani, and A. R. Bodmer, Pramana **51**, 421 (1998)
[11] E. Hiyama, M. Isaka, T. Doi, and T. Hatsuda, Phys. Rev. C **106**, 064318 (2022), arXiv: 2209.06711[nucl-th]
[12] E. Hiyama, K. Sasaki, T. Miyamoto, T. Doi, T. Hatsuda, Y. Yamamoto, and T. A. Rijken, Phys. Rev. Lett. **124**, 092501 (2020), arXiv: 1910.02864[nucl-th]
[13] E. Hiyama and K. Nakazawa, Ann. Rev. Nucl. Part. Sci. **68**, 131 (2018)
[14] Y. Tanimura, H. Sagawa, T.-T. Sun, and E. Hiyama, Phys. Rev. C **105**, 044324 (2022)
[15] E. Hiyama, M. Isaka, M. Kamimura, T. Myo, and T. Motoba, Phys. Rev. C **91**, 054316 (2015), arXiv: 1504.07735[nucl-th]
[16] J. Lee, Q. Wu, Y. Funaki, H. Zong, and E. Hiyama, Few-Body Systems **60** (2019).
[17] Q. Wu, Y. Funaki, E. Hiyama, and H. Zong, Phys. Rev. C **102**, 054303 (2020)
[18] Q. Wu, Y. Funaki, and X. Chen, Phys. Rev. C **107**, 014317 (2023), arXiv: 2210.04601[nucl-th]
[19] T. Myo and E. Hiyama, Phys. Rev. C **107**, 054302 (2023), arXiv: 2304.07662[nucl-th]
[20] H. Mei, K. Hagino, J. M. Yao, and T. Motoba, Phys. Rev. C **90**, 064302 (2014), arXiv: 1406.4604[nucl-th]
[21] J. Hu, Y. Zhang, and H. Shen, J. Phys. G **49**, 025104 (2022), arXiv: 2104.13567[nucl-th]
[22] R. Xu, C. Wu, and Z. Ren, Nucl. Phys. A **933**, 82 (2015)
[23] K. Hagino and J. M. Yao, Int. Rev. Nucl. Phys. **10**, 263 (2016), arXiv: 1410.7531[nucl-th]
[24] B.-N. Lu, E.-G. Zhao, and S.-G. Zhou, Phys. Rev. C **84**, 014328 (2011)
[25] Z.-X. Liu, C.-J. Xia, W.-L. Lu, Y.-X. Li, J. N. Hu, and T.-T. Sun, Phys. Rev. C **98**, 024316 (2018)
[26] S.-H. Ren, T.-T. Sun, and W. Zhang, Phys. Rev. C **95**, 054318 (2017)
[27] X.-R. Zhou, A. Polls, H.-J. Schulze, and I. Vidaña, Phys. Rev. C **78**, 054306 (2008)
[28] H.-J. Schulze, M. Thi Win, K. Hagino, and H. Sagawa, Progress of Theoretical Physics **123**, 569 (2010)
[29] H.-J. Schulze and E. Hiyama, Phys. Rev. C **90**, 047301 (2014)
[30] J. Guo, C. F. Chen, X.-R. Zhou, Q. B. Chen, and H.-J. Schulze, Phys. Rev. C **105**, 034322 (2022)
[31] Y.-X. Liu, C. F. Chen, Q. B. Chen, H.-T. Xue, H.-J. Schulze, and X.-R. Zhou, Phys. Rev. C **108**, 064312 (2023)
[32] C. F. Chen, Q. B. Chen, X.-R. Zhou, Y. Y. Cheng, J.-W. Cui, and H.-J. Schulze, Chinese Phys. C **46**, 064109 (2022)
[33] C.-F. Chen, Q.-B. Chen, X.-R. Zhou, and Y.-Y. Cheng, Symmetry **13**, 10 (2021)
[34] D. Baye, P.-H. Heenen, and M. Libert-Heinemann, Nucl. Phys. A **291**, 230 (1977)
[35] P. Descouvemont and D. Baye, Rep. Prog. Phys. **73**, 036301 (2010)
[36] D. Bai and Z. Ren, Phys. Rev. C **101**, 034311 (2020)
[37] D. Bai and Z. Ren, Phys. Rev. C **103**, 014612 (2021)
[38] H. Zhang, D. Bai, Z. Wang, and Z. Ren, Phys. Rev. C **107**, 064304 (2023)
[39] J. Aguilar and J. M. Combes, Commun. Math. Phys. **22**, 269 (1971)
[40] E. Balslev and J. M. Combes, Commun. Math. Phys. **22**, 280 (1971)
[41] S. Aoyama, T. Myo, K. Katō, and K. Ikeda, Prog. Theor. Phys. **116**, 1 (2006)
[42] T. Myo, Y. Kikuchi, H. Masui, and K. Katō, Prog. Part. Nucl. Phys. **79**, 1 (2014), arXiv: 1410.4356[nucl-th]
[43] H. Zhang, D. Bai, Z. Wang, and Z. Ren, Phys. Rev. C **105**, 054317 (2022)
[44] H. zhang, D. Bai, and Z.-Z. Ren, Chinese Physics C (2024).
[45] X. Zhang, (2024a), arXiv: 2408.03309[nucl-th].
[46] X. Zhang, (2024b), arXiv: 2411.06712[nucl-th].
[47] T. Berggren, Nuclear Physics A **109**, 265 (1968)
[48] N. Michel, W. Nazarewicz, M. Ploszajczak, and T. Vertse, J. Phys. G **36**, 013101 (2009), arXiv: 0810.2728[nucl-th]
[49] N. Li, M. Shi, J.-Y. Guo, Z.-M. Niu, and H. Liang, Phys. Rev. Lett. **117**, 062502 (2016)
[50] Y.-J. Tian, T.-H. Heng, Z.-M. Niu, Q. Liu, and J.-Y. Guo, Chinese Physics C **41**, 044104 (2017)
[51] X.-N. Cao, Q. Liu, Z.-M. Niu, and J.-Y. Guo, Phys. Rev. C **99**, 024314 (2019)
[52] S.-Z. Xu, S.-S. Zhang, X.-Q. Jiang, and M. S. Smith, Nucl. Sci. Tech. **34**, 5 (2023)
[53] T. Busch, B.-G. Englert, K. Rzazewski, and M. Wilkens, Found. Phys. **28** (1998).
[54] M. Lüscher, Nucl. Phys. B **354**, 531 (1991)
[55] P. Guo and V. Gasparian, Phys. Rev. D **103**, 094520 (2021)
[56] X. Zhang, Phys. Rev. C **101**, 051602 (2020)
[57] X. Zhang, S. R. Stroberg, P. Navrátil, C. Gwak, J. A. Melendez, R. J. Furnstahl, and J. D. Holt, Phys. Rev. Lett. **125**, 112503 (2020)
[58] H. Zhang, D. Bai, Z. Wang, and Z. Ren, Phys. Rev. C **109**, 034307 (2024a)
[59] H. Zhang, D. Bai, Z. Wang, and Z. Ren, Phys. Lett. B **850**, 138490 (2024b)
[60] H. Zhang, D. Bai, and Z. Ren, Phys. Rev. C **110**, 034308 (2024c)
[61] C. Li, J. Yu, R. Peng, S. Lyu, and B. Long, Phys. Rev. C **104**, 044001 (2021), arXiv: 2107.12273[nucl-th]
[62] P. Guo and B. Long, J. Phys. G **49**, 055104 (2022), arXiv: 2101.03901[nucl-th]
[63] P. Guo and B. Long, Phys. Rev. D **102**, 074508 (2020), arXiv: 2007.10895[hep-lat]
[64] B. Long, J. Wang, and S. Lyu, (2017), arXiv: 1704.08935[nucl-th].
[65] A. T. Kruppa and K. Arai, Phys. Rev. A **59**, 3556 (1999)
[66] R. Suzuki, A. T. Kruppa, B. G. Giraud, and K. Katō, Progress of Theoretical Physics **119**, 949 (2008)

CPC Accepted

[67] M. T. Alley and L. D. Knutson, Phys. Rev. C **48**, 1901 (1993)
[68] R. Kamouni and D. Baye, Nuclear Physics A **791**, 68 (2007)
[69] X.-R. Zhou, H.-J. Schulze, H. Sagawa, C.-X. Wu, and E.-G. Zhao, Phys. Rev. C **76**, 034312 (2007)
[70] J. Cugnon, A. Lejeune, and H.-J. Schulze, Phys. Rev. C **62**, 064308 (2000)
[71] H.-J. Schulze and T. Rijken, Phys. Rev. C **88**, 024322 (2013)
[72] J. Margueron, E. Khan, and F. Gulminelli, Phys. Rev. C **96**, 054317 (2017)
[73] Y. Zhang, H. Sagawa, and E. Hiyama, Phys. Rev. C **103**, 034321 (2021)
[74] S. Ajimura, H. Hayakawa, T. Kishimoto, H. Kohri, K. Matsuoka, S. Minami, T. Mori, K. Morikubo, E. Saji, A. Sakaguchi, Y. Shimizu, M. Sumihama, R. E. Chrien, M. May, P. Pile, A. Rusek, R. Sutter, P. Eugenio, G. Franklin, P. Khaustov, K. Paschke, B. P. Quinn, R. A. Schumacher, J. Franz, T. Fukuda, H. Noumi, H. Outa, L. Gan, L. Tang, L. Yuan, H. Tamura, J. Nakano, T. Tamagawa, K. Tanida, and R. Sawafta, Phys. Rev. Lett. **86**, 4255 (2001)
[75] M. Bender, P.-H. Heenen, and P.-G. Reinhard, Rev. Mod. Phys. **75**, 121 (2003)
[76] E. Chabanat, P. Bonche, P. Haensel, J. Meyer, and R. Schaeffer, Nuclear Physics A **635**, 231 (1998)
[77] I. Vidaña, A. Polls, A. Ramos, and H.-J. Schulze, Phys. Rev. C **64**, 044301 (2001)

CPC Accepted